ISABE-2015-20076

Analysis of a Gas Turbine Disk Incorporating Radially Rotating Heat Pipes with a Focus on Stress Concentrations

Sina Eisenmann, Alessandro Primavera, Andreas Hupfer
Technische Universität München
Institute for Flight Propulsion
Garching, 85748, Germany
Eisenmann@lfa.mw.tum.de

Abstract

This paper presents the results of the investigation of stress concentrations induced by heat pipes incorporated in a generic turbine disk. The structural influence of various heat pipe cross sections is studied using steady-state finite element analysis. Therefore, the stress components due to rotational forces and temperature are investigated and stress concentration factors are calculated and compared with an analytical standard case. As a result of the thermally induced compressive stresses which superpose with the rotational induced tensile stresses, the resulting von Mises stresses at the notch base are significantly lower than the analytical standard case without temperature influence. It has been shown that for a heat pipe with elliptical cross section with an axial ratio of 2, the maximal von Mises stresses are up to 27% lower than for a circular cross section. Furthermore, the impact of blade masses is examined in consideration of the heat pipe position. As might be expected, the total value of the notch stresses increases in accordance with the increasing disk load without showing any high influence of the circumferential heat pipe position.

Nomenclature

a	Major axis of the ellipse	[mm]
b	Minor axis of the ellipse	[mm]
c_{hp}	Specific heat capacity of the heat pipe	[J/kgK]
d	Distance between the disk rim and the evaporator section of the heat pipe	[mm]
E_{hp}	Young's modulus of the heat pipe	[MPa]
K	Stress concentration factor	[-]
k_{hp}	Effective thermal conductivity of the heat pipe	[W/mK]
L_{hp}	Heat pipe length	[mm]
m_b	Mass of the blade	[kg]
n	Revolution speed	[rpm]
Q	Heat	[J]
r, θ, z	Components of cylindrical coordinate system	
R_a	Outer radius of the disk	[mm]
R_i	Inner radius of the disk	[mm]
T	Temperature	[K]
T_{cool}	Gas cooling temperature	[K]
T_{gas}	Gas temperature at the rim surface	[K]
x	Thickness of the disk	[mm]
α_{cool}	Heat transfer coefficient at the cooled disk surface	[W/m²K]
α_{gas}	Heat transfer coefficient at the rim surface	[W/m²K]
δ	Radius of curvature	[mm]
Δφ	Relative angle between the blade and the heat pipe	[°]
μ	Poisson's ratio	[-]
ρ_{hp}	Density of the heat pipe	[kg/m³]
σ_M	Von Mises stress	[MPa]
σ_{M*}	Von Mises stress at the disk bore of the disk without heat pipe and blade	[MPa]
σ_{max}	Maximum notch stress	[MPa]
σ_{M-nom}	Reference von Mises stress	[MPa]
σ_{M-nom}	Averaged von Mises stress value along path	[MPa]

	2 for a disk without heat pipe and blade	
σ_r	Radial stress component	[MPa]
σ_z	Stress component in z-direction	[MPa]
σ_φ	Hoop stress component	[MPa]
$\sigma_{\varphi\text{-nom}}$	Averaged, rotational induced hoop stress value along path 2 for a disk without heat pipe and blade	[MPa]
$\sigma_{\varphi\text{-rot}}$	Hoop stress component induced by rotational forces	[MPa]
$\sigma_{\varphi\text{-temp}}$	Temperature induced hoop stress component	[MPa]
ω	Angular velocity	[1/s]

Introduction

A key prerequisite for a further increase in efficiency and thrust to weight ratio of modern gas turbine aero engines is an increase in turbine inlet temperature. This temperature is limited by the temperature tolerance of the used blade and disk material for a certain number of cycles. Turbine disks are loaded by high rotational forces and hot temperatures. The typical disk failure is due to low cycle fatigue [1]. One possibility to control thermal stresses and reducing the temperature at the disk rim may be inserting heat pipes into the disk material [2, 3, 4, 5]. This heat pipes have a high thermal conductivity which exceeds the thermal conductivity of copper by 60-100 times [6]. This enables a fast heat transfer from the hot rim section to cooler areas of the disk and leads to a significant cooling effect at the rim [2, 5]. Furthermore, the changed radial temperature profile inside the disk influences the induced thermal stresses. This leads to a lower stress level in various areas of the disk [2, 3, 4].
Figure 1 illustrates the operational schematic of a heat pipe under centrifugal forces. A two-phase working fluid is located inside a closed container. The heat Q is transferred to the fluid at the evaporator section and causes a phase change and therefore a local increase in pressure. This pressure gradient causes the vapor to flow to the cooler condenser section and condensates by releasing the heat Q. Due to the high centrifugal forces inside the disk, the liquid phase is pushed back to the condenser section, so no additional wick structure is needed.
For turbine applications, working fluids such as sodium or potassium are suitable [5]. The performance of this kind of heat pipes has been subject to extensive analytical and experimental studies [6, 7, 8, 9] and the investigations of Cao et al. [7, 9] show that they are suitable for turbomachinery applications.

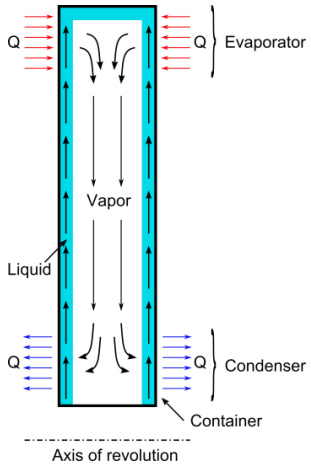

Figure 1. Schematic of a heat pipe under centrifugal forces [9, 10, 11]

Nevertheless, the cavity of the heat pipe creates notch stresses which may reduce the durability of the disk material. Former investigations of Eisenmann et al. [2, 3] have shown that there are high stress concentrations in the disk material around the condenser ending and at the lateral sides along the heat pipe length. Due to the probably high impact on the durability of the turbine disk, it is evident to further investigate and minimize these stresses. This paper examines the influence of different heat pipe cross sections on the stress peaks and compares the values with analytical stress concentration factors. Therefore steady-state finite element simulation is used. Furthermore, the generic disk model of former investigations [2, 3] is extended by a generic blading to consider the impact of the additional masses on the stress level inside the disk with integrated heat pipes. The influence of the circumferential position of the heat pipe in relation to the blade is additionally investigated.

Theory

To understand the notch stresses induced by the inserted heat pipe, it is essential to recognize the stress components inside a rotating disk with a central hole in general. Figure 2 illustrates such a disk with an inner radius R_i, an outer radius R_a and a thickness x, which rotates with a constant angular velocity ω. On the right, the resulting radial and hoop stress components σ_r and σ_φ inside the disk are plotted qualitatively over the radius r. As can be extracted, the hoop stresses are dominant, especially at the high loaded inner radius. Without thermal influence, these stress contributions could be calculated by Equation 1 and 2 [12, 13]. For a detailed analysis of the stress components of the used generic disk shape compare Eisenmann et al. [2].

$$\sigma_r = \frac{\rho \cdot \omega^2 \cdot (3+\mu)}{8}\left(R_i^2 + R_a^2 - \frac{R_i^2 \cdot R_a^2}{r^2} - r^2\right) \qquad \textbf{Eq. 1}$$

$$\sigma_\varphi = \frac{\rho \cdot \omega^2 \cdot (3+\mu)}{8}\left(R_i^2 + R_a^2 + \frac{R_i^2 \cdot R_a^2}{r^2} - \frac{1+3\mu}{3+\mu} r^2\right) \qquad \textbf{Eq. 2}$$

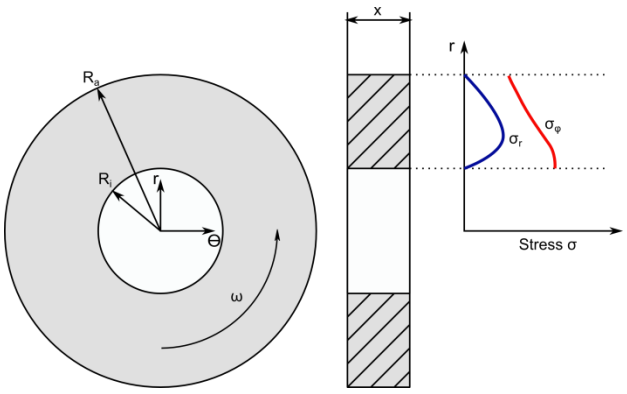

Figure 2. Schematic of stresses inside a rotating disk with a central hole [13]

For simple geometries there are analytical correlations to identify the stress distributions and maximal values due to notches [14, 15]. The stress distribution of a flat, infinite expanded thin plate with a circular or elliptic hole under uniaxial tension stress is shown in Figure 3 on the left side. The maximum stresses σ_{max} can be analytically calculated by Equation 3 [13, 14]. The used variables identify the elliptical axes a and b, the radius of curvature δ, the reference stress value σ_{nom} and the stress concentration factor K. The reference stress σ_{nom} is the resulting stress caused by the force F based on a cross section without notch (compare Figure 3, right side).

By inserting the heat pipe in the disk (compare Figure 5 and Figure 6), the resulting cavity interrupts the stress trajectories in tangential direction and induces notch stresses [2, 3]. By cutting the disk in the θ-z-plane and subsequent unwinding, the resulting cross section is approximated as a plate with an elliptic hole as described above (Figure 6).

$$\sigma_{max} = \left(1 + 2\sqrt{\frac{b}{\delta}}\right) \cdot \sigma_{nom} = K \cdot \sigma_{nom} \qquad \textbf{Eq. 3}$$

$$\delta = \frac{a^2}{b} \qquad \textbf{Eq. 4}$$

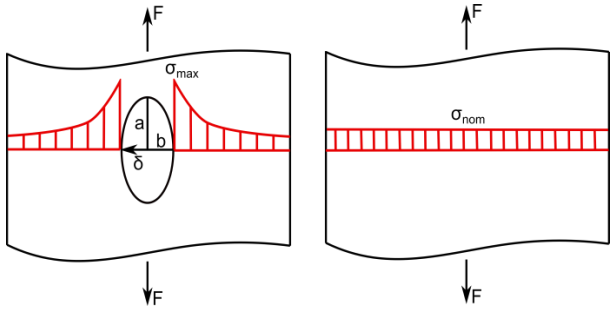

Figure 3. Schematic of the induced notch stresses due to an elliptic hole (left) and the stresses without hole (right)

Methodology

For the investigation, a three-dimensional finite element simulation is conducted by means of the commercial software Abaqus 6.13. Various model setups with and without blades are simulated. A detailed overview of the different variations is given in Table 1 and Figure 4. The variations V1-V3 focus on the impact of the heat pipe cross section on the induced notch stresses. Therefore one circular (V1) and two elliptical (V2 and V3) cross sections are investigated. In variation V4 and V5, the impact of the blade mass and the relative position of the heat pipe to the blade are focused on. In the latter, a circular heat pipe cross section is chosen to allow comparability.

Table 1. Overview of the different heat pipe variations

Variation	Blade	Δφ [°]	a/b	δ	d [mm]
V1	-	0	1	1	4
V2	-	0	3/2	1.84	4
V3	-	0	2/1	2.83	4
V4	X	0	1	1	4
V5	X	3	1	1	4

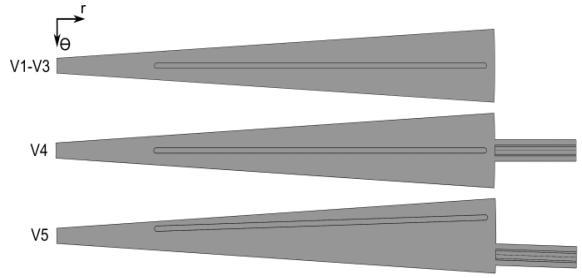

Figure 4. Overview of the different heat pipe setups

A schematic of the principal model setup is shown in Figure 5 and Figure 6. Due to symmetry concerns only a sector of 6 degrees is simulated. The outer radius of the disk R_a measures 265 mm and the inner radius R_i 54 mm. The blade has a simple hollow design and has a mass m_b of 0,032 kg.

Due to former investigations [2, 3], the heat pipe length L_{hp} has been chosen to 160 mm. The evaporator end keeps the distance d of 4 mm to the rim. The relative angle Δφ indicates the angle between the axis of the blade and the heat pipe. Therefore, the value of Δφ is 0° if the heat pipe is located underneath the blade (V4) and 3° if the heat pipe is located between two blades (V5). For the sector boundaries, the cyclic symmetry interaction is used. Furthermore, there is a symmetry of the assembly to the r-θ-plane which is modeled by locking the degree of freedom in z-direction (compare Figure 7). To investigate the influence of the heat pipe shape on the induced notch stresses in the disk material, three different cross sections are simulated. Based on a circular cross section with a radius of 1 mm (V1), two elliptical cross sections are selected. Keeping the cross section area constant, the relation of the major axis a to the minor axis b of the ellipse has been set to 3/2 (V2) and 2/1 (V3). The major axis a is located in the r-θ-plane and the minor axis b is parallel to the z-axis (compare Figure 6).

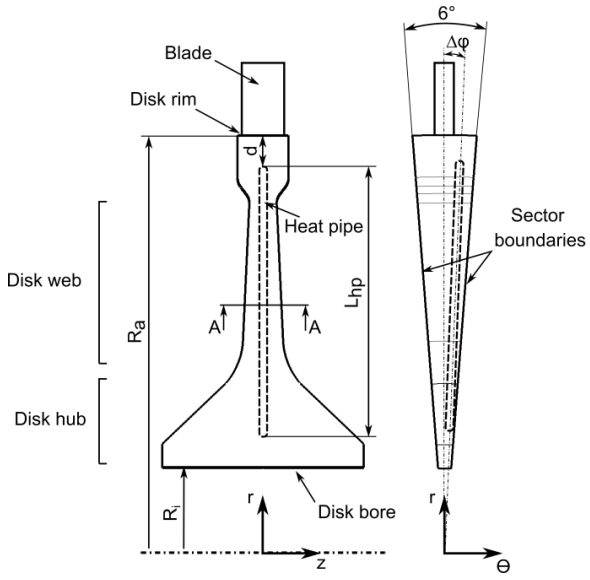

Figure 5. Schematic of the turbine disk-blade assembly incorporating a high temperature heat pipe

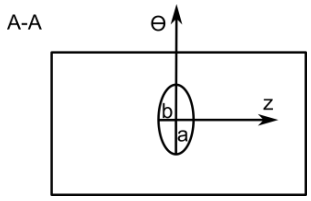

Figure 6. Sectional view A-A

Although former investigations [3] have shown that the highest stress peaks appear under transient operating conditions, a steady-state finite element analysis is performed. Due to the central aspect of the paper to identify the general reasons of the notch stresses as well as to compare various shape impacts this appears reasonable and keeps the simulation time appropriate. For variation V1-V3, the interaction of the disk material with the hot gas and cooling gas are modeled as convective boundary conditions which are schematically shown in Figure 7. The lateral sides of the disk are cooled with the cooling air T_{cool} which linearly increases over the radius from 600 K at $r = R_i$ to 1000 K at $r = R_a$ according to Equation 5.

$$T_{cool} = 1.9 \cdot r \cdot \frac{K}{mm} + 497 \ K \qquad \textbf{Eq. 5}$$

The corresponding heat transfer coefficient α_{cool} is set to 600 W/m²K. The disk rim is exposed to the hot gas temperature T_{gas} of 1250 K with the corresponding heat transfer coefficient α_{gas} of 1000 W/m²K. These values are based on former investigations [16].
To investigate the influence of the centrifugal forces, the revolution speed n has been set to 15300 rpm for all variations. The material of the disk-blade assembly used is the nickel-based super alloy Inconel 718 with temperature-dependent material properties.

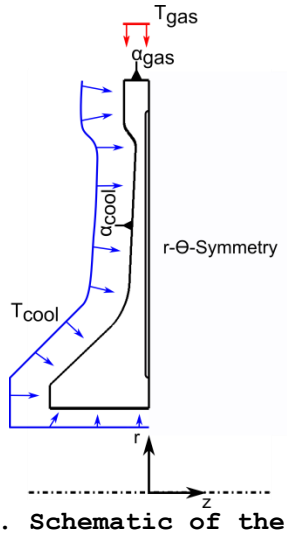

Figure 7. Schematic of the implemented boundary conditions

The heat pipe is modeled as a solid cylinder with circular (V1, V4-V5) or elliptical (V2-V3) cross section and an effective thermal conductance k_{hp} of 25000 W/mK. This value is based on the experimental investigations of Ling et al. [6] and is also used in [2, 4, 5]. In accordance with Eisenmann et al. [2], to assign isotropic material properties of the heat pipe section, it is assumed that the heat pipe is filled by one quarter liquid sodium and three quarters of sodium vapor. The different properties of the liquid and vaporized fluid are weighted by volume. Consequently the density of the heat pipe ρ_{hp} is calculated to 191 kg/m³ and the specific heat capacity to c_{hp} = 998 J/kgK. The fluid phase should not be able to transfer forces, so the Young`s modulus E_{hp} is chosen to be very low and is set to 10 MPa.
As discussed in the following, the highest notch stresses appear in the disk material next to the interface of the heat pipe. A high mesh quality is essential [17] to evaluate these stresses. Therfore a hybride mesh is used for the setup. Around the heat pipe, a structured mesh in the shape of a hollow cylinder is used, which is highly refined in direction to the interface. An example of the mesh is shown in Figure 8. The detail shows the structured mesh in the area of the condenser ending. The whole mesh consists of around 500,000 second-order elements.

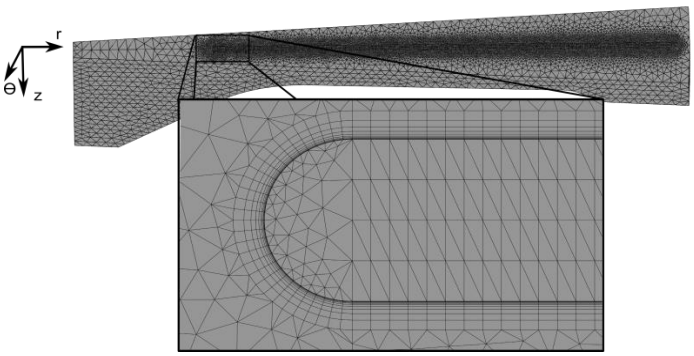

Figure 8. View of the mesh; the detail shows the condenser ending

Results

Former investigations [3] have shown that the highest stresses appear at the notch base in the r-z-plane along path 1, which is shown in Figure 9. To normalize the stress values, the maximum von Mises stress value σ_{M*} at the disk bore of the disk without heat pipe and blade is used.

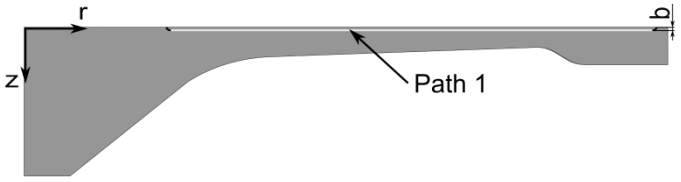

Figure 9. Location of path 1

In Figure 10 a contour plot of the von Mises stress distribution of variation V1 is given. For a detailed analysis of the appearing stresses in the disk material also compare [2, 3]. The detail shows a cut parallel to the r-θ-plane and locates path 2 which runs from the heat pipe disk

interface to the disk surface. As discussed in the following, the highest stresses appear at 0.25 of normalized path length of path 1, therefore path 2 is located at this radial coordinate. At the interface, the crescent-shaped notch stresses in the disk material are visible. These stresses result due to temperatures and rotational forces. Therefore, as shown in Figure 2, the hoop stress component σ_φ is dominant. In Figure 11, three contour plots of the normalized hoop stress components induced by rotational forces (a), temperatures (c), and the combination (b) are shown. It is visible that the notch stresses in (a) are higher than in (b). This is due to the negative temperature gradient from the heat pipe to the cooled disk surface which leads to thermal compression stresses (c). These stresses superpose with the high tension stresses due to rotational forces and lead to lower hoop stress values in the notch area in the combined load case.

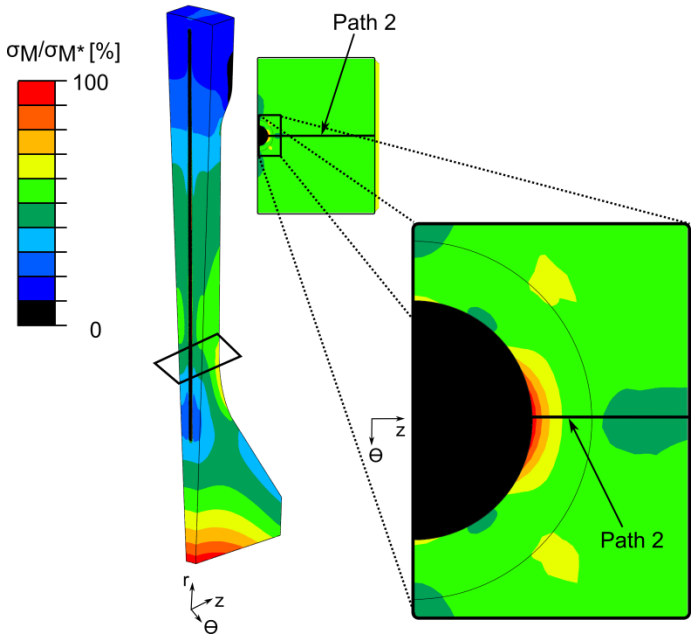

Figure 10. Contour plot of the normalized von Mises stresses of variation V1; the detail shows a cut parallel to the r-θ-plane and the location of path 2

The absolute value of the various stress components at the notch base depends on the radial positon. Figure 12 shows the normalized hoop stress components σ_φ due to temperature $\sigma_{\varphi\text{-temp}}$ and rotational forces $\sigma_{\varphi\text{-rot}}$ as well as the component of the combined load case σ_φ along path 1. It is visible, that the hoop stress $\sigma_{\varphi\text{-rot}}$ in the notch base is maximal at a normalized path length of 0.3 reaching high stress values of up to 137% of σ_{M^*}. With increasing radius, this stress component drops according to the nominal surrounding stress level (compare Figure 2 and Eisenmann et al. [2]). The stresses induced by temperature are negative over the whole length of the heat pipe. These compressive stresses increase with increasing path length due to the temperature distribution inside the disk material (compare [2]). The stresses of the combined load case are in between both curves and have their maxima at around 0.25 of normalized path length.

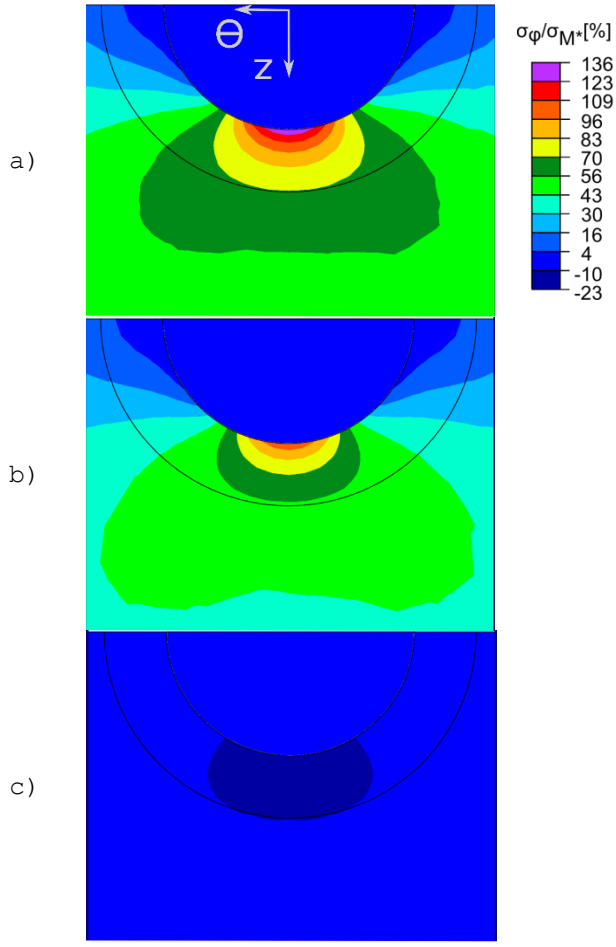

Figure 11. Contour plot of the normalized hoop stresses in cut parallel to the r-θ-plane due to rotational forces (a), temperature (c) and combination (b)

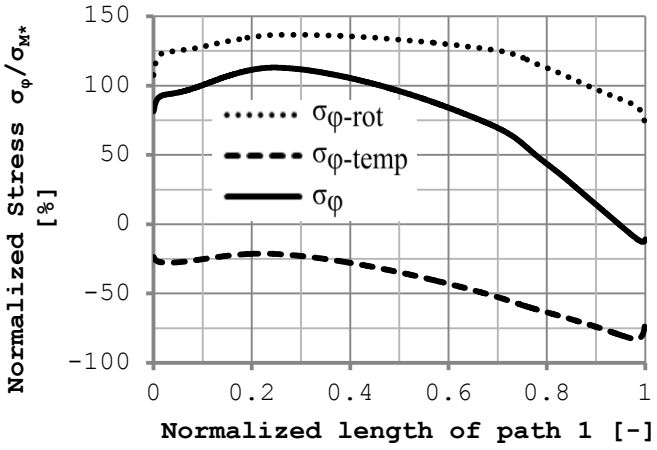

Figure 12. Distribution of the normalized hoop stress components due to temperature and rotational forces and the combined load case of variation V1 along path 1

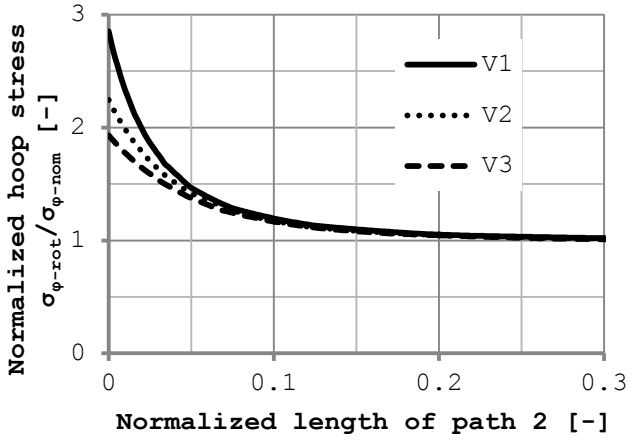

Figure 13. Characteristic of the normalized hoop stress component induced by rotational forces of variation V1-V3 along path 2

To determine and to compare the stress concentration factors for the different heat pipe cross sections with the analytical case (Figure 3, Equation 3), the hoop stress components due to rotational forces $\sigma_{\varphi\text{-rot}}$ are relevant. Figure 13 shows the characteristics of $\sigma_{\varphi\text{-rot}}$ normalized on the nominal hoop stress $\sigma_{\varphi\text{-nom}}$ for the various heat pipe shapes of variation V1-V3 along path 2. The value of $\sigma_{\varphi\text{-nom}}$ has been identified by averaging the hoop stress values due to rotational forces along path 2 for a reference disk without heat pipe and blade. It can be seen that at the heat pipe interface, at normalized path length 0, the stresses peak according to Figure 3 and decrease with increasing path length. The value $\sigma_{\varphi\text{-nom}}$ is already reached at 0.3. By increasing the axial ratio a/b of the ellipse, the radius of curvature lowers and the maximum stress σ_{max} decreases in accordance with Equation 3. The first two columns of Table 2 list the analytical and simulative calculated values of the stress concentration factor K. The values display good coverage in general. Differences are related to the assumption of the infinite expanded thin plate in contrast to the finite width of the disk and the curved cross-section.

The resulting curves of the normalized von Mises stresses $\sigma_M/\sigma_{M\text{-nom}}$ of the combined load case along path 2 are plotted in Figure 14. Therefore, $\sigma_{M\text{-nom}}$ is calculated equivalent as $\sigma_{\varphi\text{-nom}}$. Due to the temperature influence, the maximum values, which are also presented in Table 2, are considerably lower than in Figure 13.

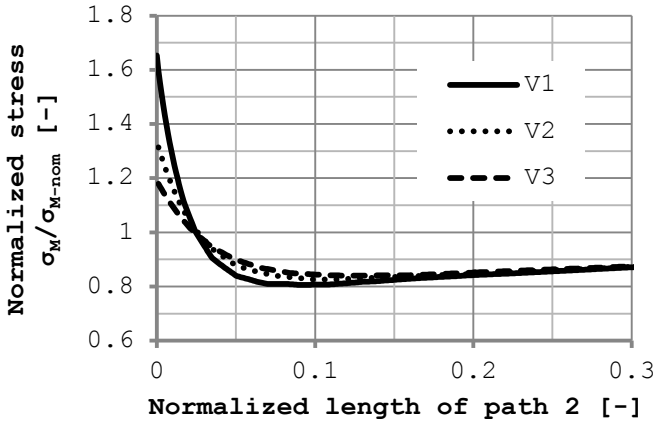

Figure 14. Characteristic of the normalized von Mises stress of the combined load case of variation V1-V3 along path 2

To obtain an overview of the total height of the notch stresses, Figure 15 shows the characteristics of the normalized von Mises stresses σ_M/σ_{M*} of variation V1-V3 along path 1. Comparing the characteristic of variation V1 with the characteristic of σ_φ in Figure 12, it is apparent that both curves are very similar, which signifies

the high influence of σ_φ in the von Mises stresses.
The maximum von Mises stress of V1 is 2% higher than σ_{M*}. Comparing the curves of the von Mises stresses of variation V2 and V3 it can be seen that they reach only 82 and 73% of σ_{M*} and are therefore significantly lower than V1 in an area of 0-0.7 of normalized path length. This is a result of the elliptic cross section of the heat pipe for these two variations. Therefore the maximum stress value, which locally exceeds σ_{M*} for V1, can be efficiently lowered to a maximum of around 73% of σ_{M*} for V3. The maximum ratio of σ_M/σ_{M*} is also given in Table 2.

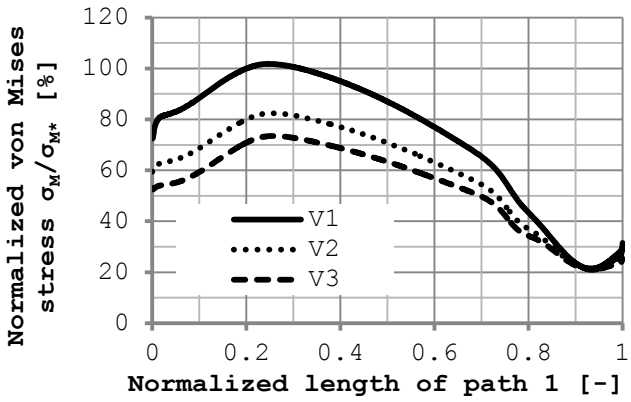

Figure 15. Characteristic of normalized von Mises stresses along path 1 for V1-V3

Table 2. Overview of the resulting stress concentration factors

	V1	V2	V3
K analytical calculation by Eq.3	3	2.33	2
K simulative results $\sigma_{\varphi\text{-rot}}/\sigma_{\varphi\text{-nom}}$	2.85	2.25	1.93
$\sigma_M/\sigma_{M\text{-nom}}$	1.65	1.34	1.2
σ_M/σ_{M*}	1.02	0.82	0.73

Another area of increased stresses due to the heat pipe implementation is located at the condenser ending. In Figure 16 a contour plot of the normalized von Mises stresses of the combined load case at the condenser ending of variation V1 is plotted. The stress peak in the disk material close to the heat pipe is visible. The characteristics of the normalized stress components σ_φ , σ_r and σ_z as well as the von Mises stresses σ_M along path 3, which is shown in Figure 16, are plotted in Figure 17. The radial stress component σ_r is maximal at around 0.2 of normalized path length and decreases to almost zero at 1.0 due to the very small ability of the heat pipe to transfer forces. For the same reason, the hoop stress component starts at zero and reaches its maximal value at the heat pipe axis at a normalized path value of 1.0. The negative values of the stresses in z-direction are nearly constant at around 0.3 and are temperature induced. The resulting von Mises stresses reach 65% of σ_{M*} at a normalized path value of 1.0.

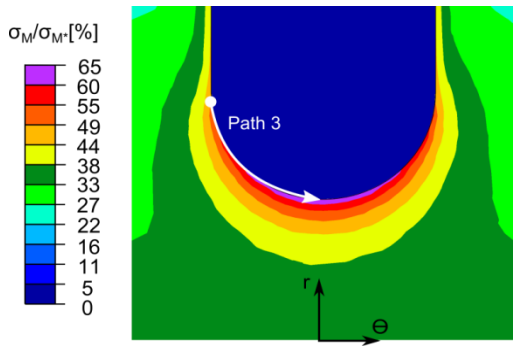

Figure 16. Contour plot of normalized von Mises stresses at the condenser ending of V1

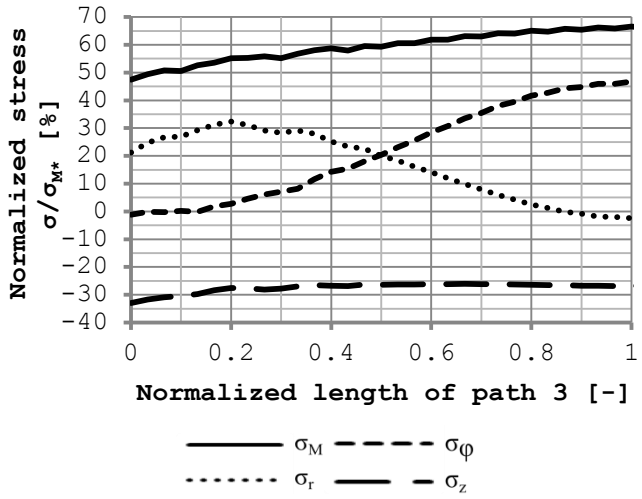

Figure 17. Characteristics of normalized stresses along path 3

In the following, the influences of the circumferential position of the heat pipe are presented. For the model setup, only rotational induced stresses are investigated, therefore no temperature

boundary conditions are modeled. For a first overview, Figure 18 compares the contour plot of the normalized von Mises stresses $\sigma_{M\text{-}rot}$ due to rotational forces for variation V4 and V5.
The characteristics of the normalized hoop stress component due to rotational forces $\sigma_{\varphi\text{-}rot}$ for V1, V4 and V5 are plotted in Figure 19. It is apparent that the values of V4 and V5 with blade are around 5-10% higher than the values of V1 without blade. This is due to the additional mass of the blade which results in higher hoop stresses in general and therefore in higher notch stresses. Furthermore, except at the position of 0.9-1 of normalized path length, there is almost no difference between V4 and V5.

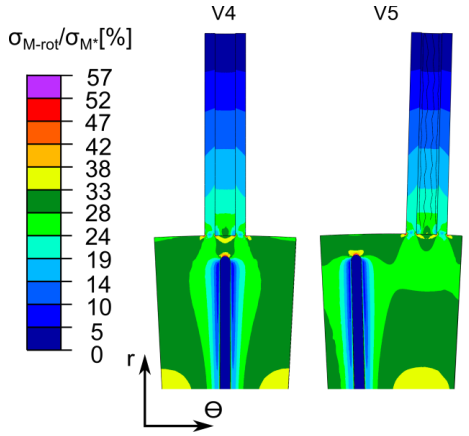

Figure 18. Contour plot of normalized von Mises stresses due to rotational forces of variation V4 and V5

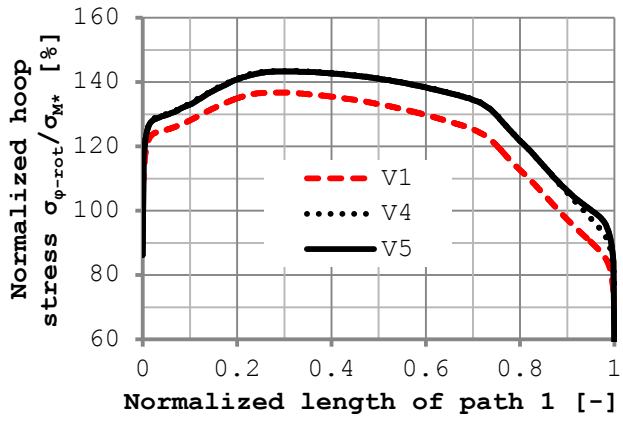

Figure 19. Normalized hoop stresses due to rotational forces along path 1 of variation V4 and V5

Conclusion and Prospects

A three-dimensional steady-state finite element analysis of a generic turbine disk with integrated heat pipes has been conducted. The maximal notch stress values due to the heat pipe were investigated. Therefore notch stress concentration factors of different heat pipe cross sections are simulatively calculated and compared to analytical correlations. The results show that due to the temperature influence the maximal von Mises stress values in the notch base are significantly lower than analytically calculated values without temperature and exceed σ_{M^*} by only up to 2%. Furthermore, by using an elliptic instead of a circular cross section with an axis ratio of 2/1, the maximum von Mises stresses are up to 27% lower than σ_{M^*}. These results show that the notch stresses induced by heat pipes can be significantly lowered by variation of their cross section. It is mentioned that these values are probably higher under transient operating conditions and need to be verified by future investigations. Furthermore, there is a need for simulative and experimental validation of the unrestricted functionality of an elliptic heat pipe under centrifugal forces for gas turbine applications.
As expected, the additional mass of the generic blade results in higher stresses inside the disk in general and increases the total height of the notch stresses as well. Furthermore, no significant influence of the circumferential position of the heat pipe in relation to the blade can be seen.
Further studies should investigate the influence of the notch stresses on the low cycle fatigue of the turbine disk and the manufacturing possibilities.

References

[1] J. Belson, "Disc failures: a cause for concern," pp. 163-166, 31. Juli 1975.

[2] S. Eisenmann, M. Mair and A. Hupfer, "Structural Analysis of a Gas Turbine Disk Containing Heat Pipes Using Finite Element Analysis," *AIAA Propulsion and Energy Conference*, July 2014, AIAA-2014-3441.

[3] S. Eisenmann, R. Körner and A. Hupfer, "Transient Simulation of a Gas Turbine Disk Incorporating Heat Pipes under Structural Aspects," in *Proceedings of ASME Turbo Expo 2015*, Montréal, Canada, 2015, GT2015-42102.

[4] S. Ding and B. Luo, "Control of Stress in Aeroengine Turbine Disk Using Radially Rotating Heat Pipe," *Journal of Thermophysics and Heat Transfer,* vol. 28, no. 3, pp. 428-439, 2014.

[5] Y. Cao and J. Ling, "Performance Simulations of a Gas Turbine Disk-Blade Assembly Employing Miniature Radially Rotating Heat Pipes," New York, 2012.

[6] J. Ling and Y. Cao, "Experimental Investiagtions of Radially Rotating Miniature High-Temperature Heat Pipes," vol. 121 (1), pp. 113-119, 2001.

[7] Y. Cao, Y. Chang and S. Won, "Analyses of Heat Transfer Limitations of Raially Rotating Heat Pipes for Turbomachinery Applications," in *32nd Thermophysics Conference AIAA-97-2542*, Atlanta, 1997.

[8] J. Ling, Y. Cao and W. Chang, "Analyses of Radially Rotating High-Temperature Heat Pipes for Turbomachinery Applications," *ASME Journal of Engineering for Gas Turbines and Power,* vol. 121, pp. 306-312, 1999.

[9] Y. Cao, "Miniature High-Temperature Rotating Heat Pipes and Their Applications in Gas Turbine Cooling," *Frontiers in Heat Pipes,* 2010.

[10] P. Dunn and D. Reay, Heat Pipes, 4th ed., Exeter: Pergamon, 1994.

[11] B. Zohuri, Heat Pipe Design and Technology, Boca Raton, Florida, USA: CRC Press, 2011.

[12] W. Pilkey, Formulas for Stress, Strain, and Structural Matrices, New York: Willey, 1995.

[13] W. Pilkey and D. Pilkey, Peterson's Stress Concentration Factors, Hoboken, New Jersey: John Wiley & Sons , 2008.

[14] H. Neuber, Kerbspannungslehre, Berlin Heidelberg New York: Springer-Verlag, 2001.

[15] G. Kirsch, "Theorie der Elasitzität und die Bedürfnisse der Festigkeitslehre," *VDI,* vol. 42, pp. 797-807, 1898.

[16] W. Erhard, "Beitrag zur Untersuchung der thermisch-mechanischen Spannungsbeeinflussung in Turbinenscheiben mittels Temperaturfeldmanipulaion," Dissertation, Technische Universität München, München, Germany, 1982.

[17] G. Müller and C. Groth, FEM für Praktiker - Band 1: Grundlagen, 71272, Renningen, Germany: expert, 2002.

[18] *Abaqus 6.13 Documentation; Analysis User's Manual,* Simulia.